Self-assembled nanoparticle patterns on carbon nanowall surface

Article *in* Physical Chemistry Chemical Physics · March 2016

DOI: 10.1039/C6CP01638C

8 authors, including:

Nikolay Suetin
Lomonosov Moscow State University
130 PUBLICATIONS **944** CITATIONS
SEE PROFILE

Lada V. Yashina
Lomonosov Moscow State University
109 PUBLICATIONS **1,025** CITATIONS
SEE PROFILE

Victor A. Krivchenko
Lomonosov Moscow State University
27 PUBLICATIONS **182** CITATIONS
SEE PROFILE

PCCP

PAPER

Self-assembled nanoparticle patterns on carbon nanowall surfaces†

N. V. Suetin,[a] S. A. Evlashin,*[a] A. V. Egorov,[b] K. V. Mironovich,[a] S. A. Dagesyan,[c] L. V. Yashina,[b] E. A. Goodilin[a] and V. A. Krivchenko[a]

Cite this: *Phys. Chem. Chem. Phys.*, 2016, **18**, 12344

Received 10th March 2016,
Accepted 31st March 2016

DOI: 10.1039/c6cp01638c

www.rsc.org/pccp

We observed that thermally treated carbon nanowalls serve efficiently as templates governing the formation of quasiperiodic patterns for nanoparticles deposited. Here we report self-assembled quasi-regular structures of diverse nanoparticles on a freestanding multilayer graphene-like material, *i.e.* carbon nanowalls. Metallic (Ag, Al, Co, Mo, Ni, and Ta) and semiconductor (Si) nanoparticles form coaxial polygonal closed loop structures or parallel equidistant rows, which evolve upon further deposition into bead-like structures and, finally, into nanowires. Weakly bonded nanoparticles decorate atomic steps, wrinkles and other extended defects on the carbon nanowalls as a result of anisotropic diffusion of atoms or clusters along the hexagonal sp^2-carbon network followed by their aggregation and agglomeration. The decorated carbon nanowalls are found to be promising materials for surface enhanced Raman scattering (SERS) analysis.

1. Introduction

Within the past decade, an impressive variety of potential applications have been proposed for graphene and graphene-based materials; among them, graphene implementation into various nanocomposites has become the most rapidly developing area. In particular, such carbon materials play a prominent role as unique building blocks for new nanostructured systems. In such systems, graphene or its derivatives serve often as templates; this provides the possibility to achieve the formation of ordered ensembles of nearly monodisperse nanoparticles of metals and semiconductors.[1–3] Such systems are characterized by unique electronic and quantum properties stemming from their low-dimensionality and periodicity, which opens up new vistas in graphene-based electronics. Another important area for their potential applications is materials chemistry since the structures are expected to be widely used for highly selective catalysis and sensing.[4]

Here, we report the first observation of a new type of quasi-ordered ensemble formed by metallic (Ag, Al, Co, Mo, Ni, and Ta) or semiconductor (Si) nanoparticles, *i.e.* circular patterns and bead-like structures on the surface of carbon nanowalls (CNWs) that are vivid examples of graphene-based materials obtained from hydrocarbon plasma.[5] A typical CNW film consists of densely packed arrays of freestanding micron-size flakes of multilayer graphene with a dominating vertical orientation and a chaotic lateral arrangement. The thickness of each flake may vary from several graphene layers to tens of nanometers. Their catalyst-free growth mechanism and, hence, surface morphology are found to be rather different from those for single-layer and multilayer graphene grown on metals and SiC.[6–8] Recently CNWs were suggested as the templates for a wide class of nanostructured materials[9] that are promising for fabricating sensors,[10] micro-supercapacitors,[11] fuel cells,[12] *etc.*

In the present work, we discuss phenomenologically the mechanism of the nanoparticle self-assembly on the carbon nanowalls in its relation to the surface structure.

2. Materials and methods

The CNW films were grown on polished p-doped 460 μm thick Si(100) wafers with an area of 1 cm^2. All substrates were preliminary ultrasonically treated in a diamond powder (Micron 5) suspension for 5 min to assist the carbon film nucleation. Further on, the substrates were washed in distilled water and dried. The CNW films were grown in the plasma of dc glow discharge in a mixture of hydrogen and methane. The working mixture pressure was 50 Torr at the moment of discharge ignition and was gradually increased up to 150 Torr. The substrate temperature during growth was about 750 °C. The details of the experiment are described elsewhere.[5,6]

After the process of CNW film growth samples were transferred to another facility where deposition of nanoparticles has

[a] *Skobeltsyn Institute of Nuclear Physics, Moscow State University, 119991 Moscow, Russia. E-mail: stevlashin@gmail.com; Fax: +7 495-9395175*
[b] *Department of Chemistry, Moscow State University, 119991 Moscow, Russia*
[c] *Department of Physics, M.V. Lomonosov Moscow State University, 119991 Moscow, Russia*

† Electronic supplementary information (ESI) available. See DOI: 10.1039/c6cp01638c

been carried out by means of the magnetron sputtering method in an Ar atmosphere. The following parameters were used for magnetron deposition: a gas pressure of 5×10^{-2} Torr; a substrate temperature during deposition of 250–300 °C; a deposition rate of 0.8 nm s^{-1}; a period of deposition of 10–30 s.

It should be noted that we studied CNWs with a height less than 1.5 μm. This allowed us to obtain samples with uniform distribution of nanoparticles over the whole CNW surface.

All samples were studied by means of SEM (Carl Zeiss Supra 40 system), TEM (model JEM 2100F (UHR/Cs) with acceleration voltage – 200 kV), and Raman spectroscopy (Renishaw InVia Reflex spectrometer using a 514 nm wavelength laser with a power of 30 mW subsequently decreased in the SERS experiments). The samples for TEM were grown on a stainless mesh. XPS measurements were performed at RGBL beamlines at BESSY II synchrotron facility (Berlin, Germany). The samples were preliminary annealed at 400 °C for 30 min to remove the adventitious pollutions.

3. Results and discussion

From microscopic studies, we found several types of nanoparticle patterns decorating the nanowall surface. The first of them is illustrated in Fig. 1a. Here, one can see a typical SEM image of the CNW surface covered with molybdenum nanoparticles, as an example; the nanoparticles are randomly distributed within "coaxial" closed loops. The mean distance between the nanoparticles is about 2–7 nm. From the high-resolution cross-sectional TEM image presented in Fig. 1b it is clearly seen that the particles decorate the atomic steps or graphene layer edges on the nanowall surface. Such a nanoparticle arrangement seems to stem from the nanowall thickness variation with their height resulting in a wedge cross-section of the nanowall, which in turn is explained by different growth rates of outer and inner graphene layers.[5]

A further investigation of the CNWs covered with nanoparticles reveals an alternative type of structure that can be hardly explained by the influence of atomic steps. For all metals and Si, we found structures with different geometry. A common example of such structures is presented in Fig. 2 and in the ESI.† Thus the nanoparticles form randomly oriented clusters on a CNW surface if deposition is carried out at room temperature (Fig. 2a). However an increase in substrate temperature during deposition up to 250–300 °C leads to the formation of well-ordered linear bead structures with a mean spacing of 6–15 nm, as clearly seen from Fig. 2b. An increase in the amount of material deposited onto the nanowall surface results in coalescence of separate nanoparticles (Fig. 2c).

We found from the microscopic observations the following features of the patterning phenomena:

(i) Linear bead structures are parallel to the nanowall edges, and if the nanowall edge changes its direction, the linear structures follow the new direction as well (Fig. 2 and Fig. S5, S6, ESI†). On a larger scale, the patterns have the 6-fold symmetry.

(ii) The flatness of carbon nanowalls or deviation from planarity has a minor effect on self-ordering of nanoparticles.

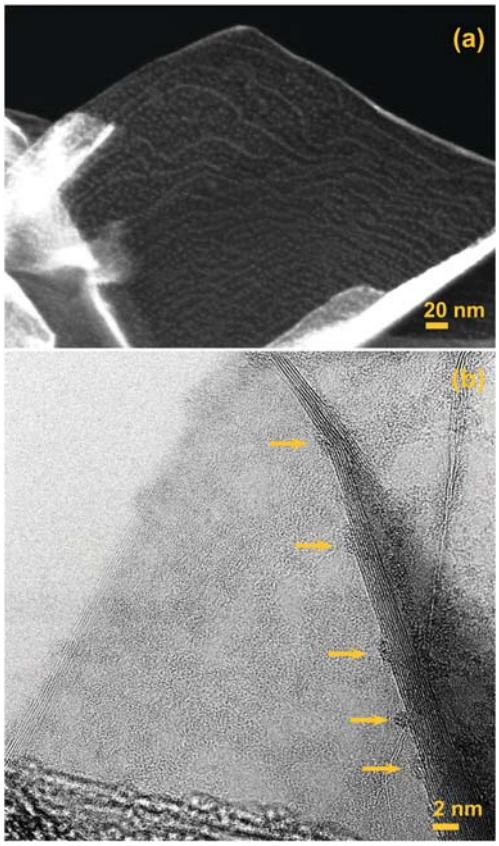

Fig. 1 (a) SEM image of a CNW covered with Mo nanoparticles and (b) TEM image of Mo particles (indicated with arrows) anchored on edges of graphene layers.

Even in exceptional cases, when the nanowall has a pronounced curvature, the linear structures are not greatly distorted as demonstrated in Fig. 2c and Fig. S6–S8 (ESI†).

(iii) No shadow effect was observed (*i.e.* there are no nanowall surfaces or areas uncovered with particles in the vicinity of another nanowall). It is, therefore, evident that nanoparticles nucleate, grow and assemble into the patterns uniformly on the entire CNW (see ESI†).

(iv) There is no preferential crystallographic (epitaxial) orientation of the nanoparticles. Almost all of the nanoparticles demonstrate typically random orientations of their lattice with respect to each other and, in turn, to the underlying graphene structure as evident from Fig. S9 (ESI†).

(v) All materials used surprisingly show very similar behavior. In addition, XPS analysis shows no chemical bonding of nanoparticles to carbon, *i.e.* no carbide formation (Fig. S12, ESI†).

The current understanding of nanoparticle assembling on sp^2-carbon materials is fully based on the concept of the predominant role of the surface layer morphology in its correlation with the subsurface layer arrangement. For the well-studied graphene obtained by CVD on metallic substrates, the nanoparticle self-assembly is usually associated with the surface roughness, namely with the presence of the Moiré pattern arising due to the misorientation between graphene layers, *i.e.* their rotation relative to each other or relative to the substrate

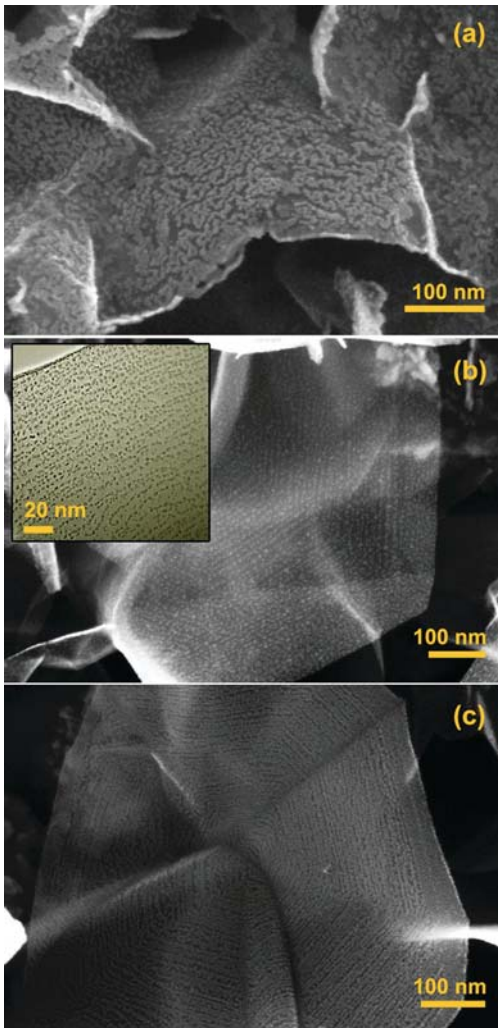

Fig. 2 SEM images of a CNW decorated with Si nanoparticles after 30 seconds of deposition at room temperature on the as-grown CNWs (a); after 20 seconds (b) and 40 (c) seconds of deposition at temperatures of 250–300 °C; inset: low resolution TEM image of decorated CNWs.

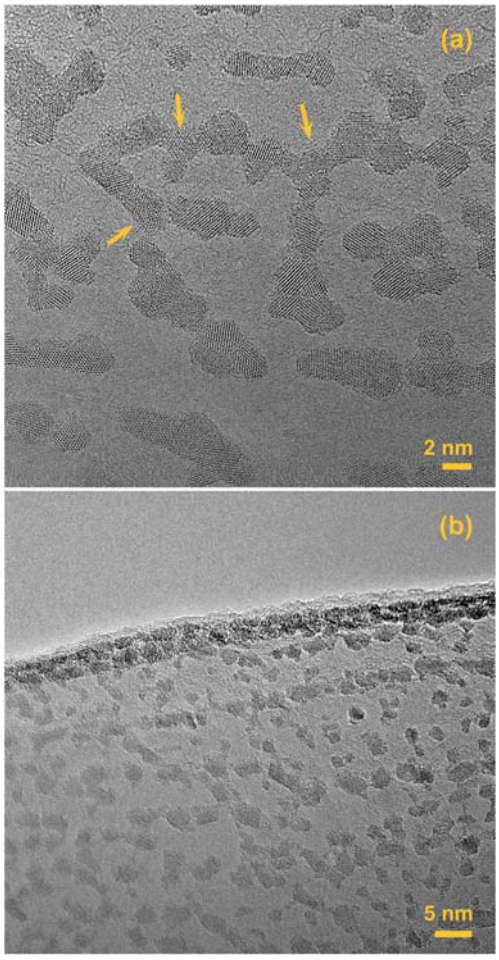

Fig. 3 (a) TEM image of X-like Mo clusters (indicated with arrows) on a CNW surface and (b) TEM image of the linear arrangement of Mo clusters oriented parallel to the CNW edge.

surface[13,14] or due to surface corrugation.[15] The period of the two-dimensional Moiré lattice directly depends on the rotation angle. In addition, relative strain between the graphene layers has a certain impact on the Moiré lattice parameter as well.[16]

A closer look at the formation of linear arrays on the CNWs allows us to conclude that the observed self-organisation of nanoparticles occurs in a completely different way compared to the planar graphene. In particular, several growth features contradict the concept of the Moiré pattern influence on the cluster ordering. First, there are two types of nanoparticles observed on nanowalls: rows of larger, aligned nanoparticles, and smaller misoriented clusters in between, as clearly seen in Fig. 3b. The nanoparticle rows are arranged in a quasiperiodic way rather than in a strictly periodic way; if the distance between the rows becomes larger, misoriented clusters appear in the area between such two adjacent rows. Second, the Moiré structures are typical for planar graphene and would be disturbed by the curvature; in our case normally oriented graphene sheets do not introduce notable distortion to the spiral-like patterns.

Generally, the surface morphology is closely related to the growth mechanisms, which are rather different for graphene formed by hydrocarbon catalytic cracking on metals, dissolution of carbon in metals and final formation of a sp^2-network,[17] and for the CNWs. The latter grow without any catalyst in the glow discharge plasma. A nanowall grows due to a direct attachment of C_xH_y radicals, presumably CH_3, to graphene layer edges *via* the process of hydrogen abstraction.[6] The CNW growth rate is a balance between radical incorporation into the graphene edges, hydrogen etching and defect "healing".[5] Therefore, we can anticipate that due to different growth mechanisms the CNWs would have an essentially different surface morphology governing the nanoparticle pattern formation.

It is noteworthy that all the nanoparticle arrangements in linear arrays occur exclusively on the surface of CNWs annealed at temperatures higher than 200 °C. To grasp the underlying reason, we studied the structure of annealed nanowall surfaces before the nanoparticle deposition. It was revealed that annealing

at 300 °C for 30 min under vacuum conditions (10^{-6} Torr) forces the CNWs to form quasiperiodic structures resembling the patterns discussed above, which include either parallel grooves following the nanowall edges or more complex circular patterns that are further decorated with nanoparticles. Fig. 4a shows the CNW surface before annealing while Fig. 4b shows clearly that annealing leads to surface wrinkling, with the wrinkle period of about 5–15 nm. This value corresponds to the experimentally observed spacing between linear arrays of metallic nanoparticles. More complex wrinkle patterns are illustrated in Fig. 4c (correlation with the metal particle arrangement is presented in Fig. S6, ESI†). Note that the same results were obtained for CNWs annealed in an inert environment (Ar, pressure – 5 Torr). Therefore the appearance of the wrinkles is distinctly related to the post-growth heat treatment of a CNW film.

The appearance of the wrinkles may be explained by the following reasons. First, carbon nanowalls contain hydrocarbon adsorbates generated in CH_4/H_2 plasma during synthesis.[5,18] Second, there is a feasible difference in thermal expansion coefficients of single- and multilayer graphene.[19] We assume that interaction between the "bulk" nanowall and its external layer may be reduced due to hydrocarbon adsorbates located between them. Such an assumption is justified by the fact that hydrocarbons from plasma can be absorbed at carbon nanowall basal planes stimulating the processes of secondary nucleation.[5] Thus the external layer may nucleate and grow later than the primary carbon nanowall structure. In this case the outer carbon nanowall layer undergoes structural stress since the film growth occurs at a temperature of 750 °C. Further annealing of carbon nanowalls in a high vacuum stimulates desorption of hydrocarbons which is known to be occurred in the temperature range of 100–400 °C.[18] This leads to the stress relaxation of the external layer and the appearance of wrinkles. Schematically this process is presented in Fig. 4d.

We observed that the relaxation proceeds symmetrically relative to the CNW center causing the formation of typical converged 6-fold patterns presented in Fig. 2 and Fig. S7 (ESI†). In addition, the presence of the CNW structural defects and secondary nanowalls[5] results in distortions introduced to the wrinkle periodicity and, hence, the more complicated nanoparticle arrangement (Fig. S8, ESI†).

The fact that the nanoparticles form arranged linear structures during magnetron sputtering even at room temperature in the case of the preliminary annealed CNW film argues for the mechanisms proposed above (see Fig. S10, ESI†). Thus, we found evidence that nanoparticle patterns are closely related to the surface morphology, which includes the system of wrinkles appearing in a concentric arrangement from the CNW center as a result of structural relaxation promoted by the thermal treatment.

Low specificity with respect to the chemical origin of the deposited elements, weak bonding to the substrate and overall uniformity pinpoint a dominant role of lateral diffusion in the formation of such a new type of structure. The lateral diffusion seems to be anisotropic. It is confirmed by the fact that some X-like arrangements of nanoparticles with angles of 60–120° are observed with no visible defects of graphene layers nearby as shown in Fig. 3a. The formation of X-like fragments coincided

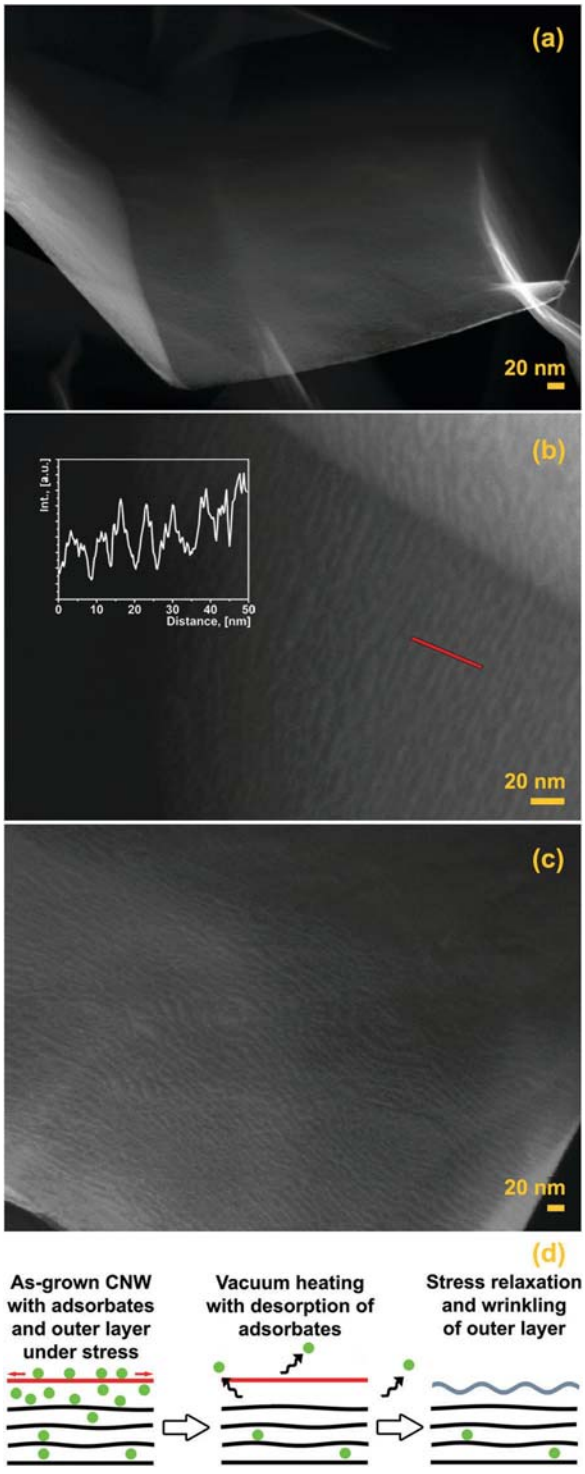

Fig. 4 SEM images of a CNW surface before annealing (a), a CNW surface after annealing in a high vacuum (10^{-6} Torr) at 300 °C for 30 minutes demonstrating the formation of linear wrinkles (b) and wrinkles with a misoriented structure (c); (d) diagram describing the wrinkle formation: the as-grown CNW contains adsorbates (green circles) and annealing in a vacuum leads to the desorption of adsorbates and stress relaxation of outer layers and wrinkle formation (marked with gray color for clarity).

with the two major orientation vectors for a hexagonal lattice of sp^2-hybridized carbons and as a consequence may lead to the sporadic formation of spiral fragments and, then, to the development of large faceted helices seen in Fig. S11 (ESI†). We observed similar behavior for different nanoparticles on the CNW surfaces, and this allows us to assume that their interaction with the nanowall basal plane is governed by van-der-Waals force with no underlying chemistry; also, no carbide formation is observed.

Most of the structures consist of two sets of nanoparticles, namely, small chaotically located small clusters and larger nanoparticles forming quasiperiodic rows and other patterns (Fig. 3b). It is also evident that the larger particles are not necessarily single crystallites but rather nanoparticle aggregates with almost random crystallographic orientation within such groups (Fig. 3 and Fig. S9, ESI†). This observation proves that there are no specific epitaxial effects acting for the CNWs and the nanoparticles.

Summing up, the dominant mechanism for the observed nanoparticle self-assembling is based on the in-plane surface diffusion of as-deposited clusters along the hexagonal sp^2-carbon network. Further geometry of aggregated structures strongly depends on the CNW surface state. We assume that the as-grown CNW surface is flat and stressed. This results in the formation of random clusters uniformly covering a CNW surface during room temperature deposition as demonstrated in Fig. 2a. The as-grown CNW surface may also contain steps and graphene layer edges which are the result of the CNW specific growth rate.[5] The appearance of such steps is of statistical nature and cannot be controlled. However they may act as anchor sites for the nanoparticles (Fig. 1).

Deposition of the nanoparticles at temperature higher than 200 °C or preliminary CNW film annealing leads to wrinkling of the external CNW layer. This results in anisotropic surface diffusion of as-deposited nanoparticles and cluster aggregation in the bottom of grooves (Fig. 2b and c).

Finally, we tested the structures under discussion for possible practical implementation as surface enhanced Raman scattering (SERS) substrates. Such substrates are predominant for SERS analyses since they have a highly developed surface and the nanostructures are certainly immobilized. This feature makes them more stable in terms of optical properties and practical use since the nanoparticles cannot detach, aggregate or redeposit. SERS spectra of the Rhodamine 6G dye and oxygenated hemoglobin were then recorded on the Ag@CNW films. The Rhodamine dye serves traditionally as a model analyte with a usual detection limit of 10^{-8}–10^{-10} M. Indeed, we revealed easily that typical Rhodamine fingerprint features (1652, 1510, 1363 cm^{-1} and other marked peaks) are already detected at 10^{-8} M concentration (Fig. 5a) evidencing that the SERS enhancement ability of the substrate is of a high level. It is also important to note that morphological features and the chemical origin of the substrates are attractive for biological object analysis since the carbon component is ready for deep modifications in terms of variation of the origin and the amount of superficial groups predetermining hydrophobicity and surface charge of the entire material. As an example, typical oxygenated hemoglobin peaks (1642, 1582, 1363, and 1123 cm^{-1}) become

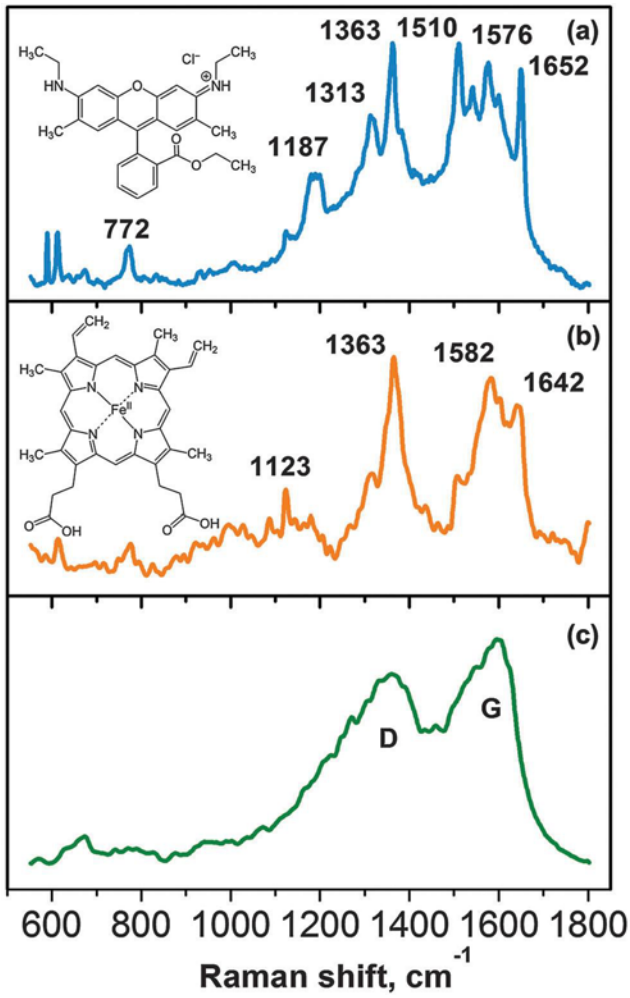

Fig. 5 SERS data of the Ag@CNW substrate using a 514 nm laser and an acquisition time of 30 s: (a) 10^{-8} M solution of Rhodamine 6G (1% laser power), (b) 10^{-6} M solution of hemoglobin (5% laser power), and (c) D and G mode peaks of the as-prepared Ag@CNW film (1% laser power).

clearly visible if 10–15 microliters of 10^{-6} M solution are dropped onto the as-prepared substrate as shown in Fig. 5b. Both the small amount of the probe and the low concentration of the protein confirm that the material demonstrates clear potential as possible active elements in SERS devices.

Obviously, some additional tasks should be solved in the future by applying the material indicated; for example, silver nanoparticles on the surface amplify greatly both the D and G modes of the CNW (Fig. 5c). The G mode corresponds to planar vibrations of carbon atoms and is typical for graphite-like materials while the D mode originates from structural defects. In the worst case, their amplification might reduce the sensitivity of SERS sensors. At the same time an additional analysis of the D and G mode features after absorption of analytes would give additional data about chemical interactions in the system and thus would strengthen the traditional SERS analysis. Thus, the present SERS results clearly demonstrate a promising outlook for the NP@CNW structure applications in the SERS analysis of various analytes.

4. Conclusions

We have demonstrated that carbon nanowall films are unique templates to form bead-like structures of metallic and semiconductor clusters and wire-like structures with an easily controlled coalescence degree. Two possible mechanisms explaining the formation of such structures may be considered. First, after the in-plane surface diffusion of adatoms, their associated atoms or even small cluster nanoparticles decorate the atomic steps, thus forming bead structures in the shape of concentric loops and hexagons or helices. Second, templating ability originates from the systematic wrinkling of the outer graphene layer due to stress relaxation during thermal treatment. This wrinkling gives rise to an equidistant wire-like structure appearance. The whole variety of structures can be realized simultaneously and in a controllable manner, therefore giving rise to new types of nanostructures with promising application features.

Acknowledgements

The authors sincerely acknowledge the support of A. Sidorov with the Raman spectra measurements. XPS measurements were performed at the RGBL beamlines at Helmholtz Zentrum Berlin BESSY II synchrotron facility (Berlin, Germany). KVM gratefully acknowledges the Russian Foundation for Basic Research (project no. 16-32-00453 mol_a). SAE gratefully acknowledges the Scholarship of the President of the Russian Federation (Project No. SP-1493.2016.4).

References

1 S. Yang, J. Dong, Z. Yao, C. Shen, X. Shi, Y. Tian, S. Lin and X. Zhang, *Sci. Rep.*, 2014, **4**, 4501.
2 P. Xu, L. Dong, M. Neek-Amal, M. L. Ackerman, J. Yu, S. D. Barber and F. M. Peeters, *ACS Nano*, 2014, **8**, 2697–2703.
3 A. T. N'Diaye, S. Bleikamp, P. J. Feibelman and T. Michely, *Phys. Rev. Lett.*, 2006, **97**, 215501.
4 Y. He, S. Su, T. Xu, Y. Zhong, J. A. Zapien, J. Li, C. Fan and S.-T. Lee, *Nano Today*, 2011, **6**, 122–130.
5 K. V. Mironovich, D. M. Itkis, D. A. Semenenko, S. A. Dagesyan, L. V. Yashina, E. Y. Kataev, Y. A. Mankelevich, N. V. Suetin and V. A. Krivchenko, *Phys. Chem. Chem. Phys.*, 2014, **16**, 25621–25627.
6 V. A. Krivchenko, V. V. Dvorkin, N. N. Dzbanovsky, M. A. Timofeyev, A. S. Stepanov, A. T. Rakhimov, N. V. Suetin, O. Y. Vilkov and L. V. Yashina, *Carbon*, 2012, **50**, 1447–1487.
7 Z. G. Cambaz, G. Yushin, S. Osswald, V. Mochalin and Y. Gogotsi, *Carbon*, 2008, **46**, 841–849.
8 G. C. Büke, G. Yushin, V. Mochalin and Y. Gogotsi, *J. Mater. Res.*, 2013, **28**, 952–957.
9 Y. H. Wu, B. J. Yang, G. C. Han, B. Y. Zong, H. Q. Ni, P. Luo and Z. X. Shen, *Adv. Funct. Mater.*, 2002, **12**, 489–494.
10 C. S. Rout, A. Kumar and T. S. Fisher, *Nanotechnology*, 2011, **22**, 395704.
11 T. M. Dinh, A. Achour, S. Vizireanu, G. Dinescu, L. Nistor, K. Armstrong and D. Pech, *Nano Energy*, 2014, **10**, 288–294.
12 B. I. Podlovchenko, V. A. Krivchenko, Y. M. Maksimov, T. D. Gladysheva, L. V. Yashina, S. A. Evlashin and A. A. Pilevsky, *Electrochim. Acta*, 2012, **76**, 137–144.
13 Y. Murata, V. Petrova, B. B. Kappes, A. Ebnonnasir, I. Petrov, Y. H. Xie, C. V. Ciobanu and S. Kodambaka, *ACS Nano*, 2010, **4**, 6509–6514.
14 K. Hermann, *J. Phys.: Condens. Matter*, 2012, **24**, 314210.
15 D. L. Miller, K. D. Kubista, G. M. Rutter, M. Ruan, W. A. de Heer, P. N. First and J. A. Stoscio, *Phys. Rev. B: Condens. Matter Mater. Phys.*, 2010, **81**, 125427.
16 J. Xhie, K. Sattler, M. Ge and N. Venkateswaran, *Phys. Rev. B: Condens. Matter Mater. Phys.*, 1993, **47**, 15835–15841.
17 A. Grüneis, K. Kummer and V. D. Vyalikh, *New J. Phys.*, 2009, **11**, 073050.
18 N. Jiang, H.-Y. Wang, H. Sasaoka, T. Deno and K. Nishimura, *Mater. Lett.*, 2010, **64**, 2025–2027.
19 W. Bao, F. Miao, Z. Chen, H. Zhang, W. Jang, C. Dames and C. N. Lau, *Nat. Nanotechnol.*, 2009, **4**, 562–566.